COMMUNICATIONS PHYSICS

ARTICLE

https://doi.org/10.1038/s42005-019-0215-8 OPEN

Quantum control of excitons for reversible heat transfer

Conor N. Murphy [1] & Paul R. Eastham[1]

Lasers, photovoltaics, and thermoelectrically-pumped light emitting diodes are thermodynamic machines which use excitons (electron-hole pairs) as the working medium. The heat transfers in such devices are highly irreversible, leading to low efficiencies. Here we predict that reversible heat transfers between a quantum-dot exciton and its phonon environment can be induced by laser pulses. We calculate the heat transfer when a quantum-dot exciton is driven by a chirped laser pulse. The reversibility of this heat transfer is quantified by the efficiency of a heat engine in which it forms the hot stroke, which we predict to reach 95% of the Carnot limit. This performance is achieved by using the time-dependent laser-dressing of the exciton to control the heat current and exciton temperature. We conclude that reversible heat transfers can be achieved in excitonic thermal machines, allowing substantial improvements in their efficiency.

[1] School of Physics, Trinity College Dublin, College Green, Dublin 2, Ireland. Correspondence and requests for materials should be addressed to P.R.E. (email: easthamp@tcd.ie)

Electron-hole pairs or excitons are essential in many different devices, forming a working medium that allows for the conversion between heat, light, and work. Important examples are photovoltaics[1] and photosynthetic reaction centres[2–4], which are thermal machines in which electron-hole pairs are created from thermal radiation at a high temperature, release heat to their surroundings at a low temperature, and thereby generate work. Thermoelectrically pumped light emitting diodes[5] and laser cooling[6–8] involve similar processes operating in reverse, with the work done on the electron-hole pairs allowing them to absorb heat from their surroundings and transfer it to the electromagnetic field. The key requirements for thermal machines such as these are high thermodynamic efficiency, η, and high power, but these requirements conflict and must be balanced against one another. For a heat engine the ultimate limit is given by the Carnot efficiency $\eta_c = 1 - T_c/T_h$, corresponding to a reversible process, but as this implies zero power a more pragmatic goal is the endoreversible efficiency at maximum power[9], or Chambadal-Novikov efficiency, $\eta_{mp} = 1 - \sqrt{T_c/T_h} < \eta_c$.

The possibility of exploiting quantum effects to enhance the performance of thermal machines is explored in recent work on quantum heat engines, covering systems including ion traps[10], electron-tunnelling devices[11–15] and micromechanical resonators[16–18]. For exciton-photon thermal machines, such as reaction centres, it has been predicted that quantum coherence can lead to enhanced performance[2–4]. However, even with such improvements their efficiency would remain well below thermodynamic limits[19]. Fundamentally this reflects the absence of methods for controlling the heat flows between excitons and their surroundings. Indeed, to reach the Carnot efficiency these heat flows should occur reversibly, i.e., over a negligible temperature difference. This requires not just control of the magnitude of the heat flows, but also of the exciton temperature.

In this article we show that controlled heat transfers between excitons and their surroundings can be achieved by driving the excitons with laser pulses. We consider quantum-dot excitons, for which quantum control[20–22] has been implemented using Rabi oscillations[23–25] and adiabatic rapid passage[26–28]. These experiments have been modelled by treating the dot as a two-level system coupled to a phonon bath, within a Born-Markov theory that accounts for the laser-dressing of the exciton in the Floquet picture[24,29]. We combine such a theory with the phase-marker approach[30] to evaluate the heat flow between excitons and phonons, when the former are driven by linearly chirped Gaussian pulses. We show that heat can be transferred from the phonon bath to the exciton, and assess the performance of a heat engine in which this forms the hot stroke. Typical pulses give efficiencies comparable to the Chambadal-Novikov result. However, for some pulses we obtain efficiencies up to 95% of the Carnot efficiency, showing that reversible heat transfers can be achieved. Our work shows that the amplitude and frequency profile of a driving laser pulse can be tuned to give complete control of exciton heat flows and exciton temperatures on picosecond timescales. This opens up the possibility of reaching thermodynamic efficiency limits in exciton-photon thermal machines.

Results

Model. We consider an InGaAs/GaAs quantum-dot, driven by an ultrafast laser pulse with a time-dependent amplitude and frequency. As illustrated in Fig. 1a, we model the dot as a two-level system, consisting of the ground state, $|0\rangle$, and a single one-exciton state, $|X\rangle$. We consider a low temperature, $T = 20$ K, and near-resonant excitation, so that other electronic states may be neglected. Furthermore, we suppose that the driving pulses are short compared with the radiative lifetime, which is generally in the nanosecond range[31], and so neglect spontaneous emission.

In this low-temperature strong-driving regime the dominant source of dissipation and dephasing is the coupling to acoustic phonons[24,32–35]. Including such phonons we have for the Hamiltonian, in the rotating-wave approximation[32],

$$\begin{aligned}\hat{H} &= \hat{H}_s + \hat{H}_b + \hat{H}_c \\ &= \Delta(t)\hat{s}_z - \Omega(t)\hat{s}_x + \sum_{\mathbf{k}} \omega_{\mathbf{k}} \hat{b}_{\mathbf{k}}^\dagger \hat{b}_{\mathbf{k}} + \hat{s}_z \sum_{\mathbf{k}} (g_{\mathbf{k}} \hat{b}_{\mathbf{k}} + g_{\mathbf{k}}^* \hat{b}_{\mathbf{k}}^\dagger).\end{aligned} \tag{1}$$

Here and in the following we set $\hbar = 1$, and use pseudospin operators, $\hat{s}_z = (|X\rangle\langle X| - |0\rangle\langle 0|)/2$ and $\hat{s}_x = (|X\rangle\langle 0| + |0\rangle\langle X|)/2$.

The terms involving summations in Eq. (1) correspond to the energy of the phonon bath, $\hat{H}_b$, and the exciton-phonon coupling, $\hat{H}_c$. The phonon bath is characterised by its spectral density, $J(\omega) = \sum_{\mathbf{k}} g_{\mathbf{k}}^2 \delta(\omega - \omega_{\mathbf{k}})$, with the super-Ohmic form $J(\omega) = (\hbar A/\pi k_B)\omega^3 e^{-(\omega/\omega_c)^2}$. We take the value of $A = 11.2$ fs K^{-1} measured by Ramsay et al.[36], and use a similar value, $\hbar\omega_c = 2$ meV, for the cut-off frequency. (The cut-off depends on the geometry of the dot[32]. Ramsay et al. report a value of 1.44 meV for dots with height 3–4 nm and base diameter 25–30 nm).

The remaining terms in Eq. (1) form the system Hamiltonian, $\hat{H}_s$, and describe the exciton driven by the laser pulse. This form is obtained by expressing the electric field of the laser in terms of its time-dependent amplitude and frequency, $E(t) = |E(t)| \cos \int \omega(t) dt$. This leads to a time-dependent Rabi frequency $\Omega(t) = d|E(t)|$, where d is the transition dipole moment, and a time-dependent exciton-laser detuning, $\Delta(t) = \omega_x - \omega(t)$. Note that $\hat{H}$ is referred to a time-dependent basis, obtained from the fixed basis (Schrödinger picture) by the unitary transformation $\hat{U}(t) = e^{i\hat{s}_z \int \omega(t) dt}$.

As in previous work on adiabatic rapid passage[26,27,37,38] we consider driving by linearly chirped Gaussian pulses, for which the Rabi splitting $\Omega(t)$ is a Gaussian of duration τ, $\Omega(t) = \Omega_0 e^{-t^2/2\tau^2}$, and the frequency $\omega(t)$ sweeps linearly in time, $\omega(t) = (\omega_x - \delta) + \alpha t$. Here α is the temporal chirp, and δ is the detuning of the pulse centre frequency below the exciton. To connect with experiments we suppose that the pulse is generated by applying a spectral chirp a to a bandwidth-limited Gaussian of pulse area Θ_0 and duration τ_0, so that[29,38–40]

$$\tau^2 = \frac{a^2 + \tau_0^4}{\tau_0^2}, \tag{2}$$

$$\alpha = \frac{a}{a^2 + \tau_0^4}, \tag{3}$$

$$\Omega_0 = \frac{\Theta_0}{\sqrt{2\pi\tau\tau_0}}.$$

Controlling heat flows. To explain how exciton-phonon heat flows can be controlled we recall the mechanism of adiabatic rapid passage using chirped pulses[21], as illustrated in Fig. 1b. This figure shows a typical example of the evolution of the dressed-state energies as the driving frequency sweeps through the resonance. These energies are given by the eigenvalues of $\hat{H}_s$, and are $\hbar\Lambda(t)/2 = \pm\hbar\sqrt{\Omega(t)^2 + \Delta(t)^2}/2$. Figure 1b shows the situation for a positively chirped pulse which crosses through the exciton resonance. In that case the lower energy state at early times in the rotating frame is the zero exciton state, whereas that at late times is the one-exciton state. The driving field splits the levels and generates an avoided crossing at $\Delta = 0$, so that the adiabatic

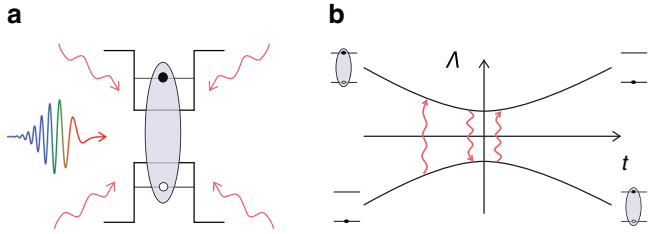

Fig. 1 Model and heat transfer mechanism. **a** Illustration of the system, consisting of a quantum-dot exciton transition driven by a laser field, and interacting with a heat bath of phonons. **b** The mechanism of heat transfer, in which phonons from the heat bath are absorbed or emitted in transitions between the laser-dressed exciton states. The graph illustrates the evolution of the dressed-state energies in a typical adiabatic rapid passage process

evolution takes the dot, initially in its ground state, into the one-exciton state.

The dressed states are coherent superpositions of the zero and one-exciton states, and are coupled together by the deformation-potential interaction with acoustic phonons[24,29,32,34,35,39,41,42]. Thus, as illustrated in Fig. 1b, a transition from the lower to the upper dressed state can occur with the absorption of a phonon of energy $\hbar\Lambda$, and vice versa with the emission of a phonon[39]. Such processes appear in a master equation for the exciton density matrix, which has been derived using standard techniques[29], with the rates $\gamma_e = \pi[n_B(\Lambda)+1]J(\Lambda)A^2/2$ for emission and $\gamma_a = \pi n_B(\Lambda)J(\Lambda)A^2/2$ for absorption. The factor $A = \Omega/\Lambda$ comes from the mixing of the zero and one-exciton states into the dressed states, and the phonon occupation function n_B and spectral density J are evaluated at the transition frequency Λ. Note that both A and Λ, and hence the rates, are time-dependent. Thus, the form of the driving pulse gives time-dependent control of the phonon emission and absorption rates. Such control, dubbed dynamic vibronic coupling[43], has been exploited in exciton and biexciton state preparation making active use of phonons[44–48].

To evaluate the heat flows in these processes we have derived and solved the equation-of-motion for the characteristic function of the heat distribution[30], following the approach used in Eastham et al.[29]. This goes beyond previous work on heat distributions[30,49] to allow for the time-dependence of the driving pulse; more generally, it allows for time-dependent system Hamiltonians, as is required to model quantum-control experiments.

Phonon cooling with chirped pulses. Figure 2 shows the predicted heat transferred from the phonons to the exciton for driving by a single chirped Gaussian pulse, with the dot starting in its ground state. The figure shows how the heat depends on the spectral chirp and pulse area, for $\tau_0 = 2$ ps, corresponding to a typical experimental value, and three values of the detuning.

Considering first the resonant case, $\delta = 0$, shown in Fig. 2a, we see that positively chirped pulses lead to heat transfer from the phonons to the exciton, i.e., a cooling of the phonon environment and a heating of the exciton. In contrast, negatively chirped and unchirped pulses lead to heating of the phonons. This can be explained in a similar way to the dependence of the exciton occupation on the sign of chirp[39]: for positive chirp the ground state of the dot is continuously connected to the lower-energy dressed state, so that only phonon absorption is possible, whereas for negative chirp it is connected to the upper-energy dressed state, and phonon emission dominates. The implications for heat transfer follow because, in both cases, the initial density matrix is thermal in the dressed-state basis. For positive chirp this thermal state has zero temperature, since only the lower level is populated, so it absorbs heat from the phonon bath at $T_{ph} = 20$ K. However, for negative chirp the initial density matrix has a negative temperature – it is inverted in the dressed-state basis – and as such the state emits heat into any positive-temperature environment[50,51].

Figure 2 also shows results for pulses that are detuned from the exciton transition, such that the frequency at the peak of the pulse lies either above the exciton (negative detuning, Fig. 2b) or below it (positive detuning, Fig. 2c). For these parameters the sign of the heat flow becomes independent of the sign of the chirp. With positive detuning the heat flow is from the phonon bath to the exciton, giving a cooling of the phonon environment, whereas for negative detuning heat flows in the opposite direction. This is because the parameters are such that the field is not significant when the frequency sweeps through the exciton, and there is no avoided crossing. Instead the sign of the detuning determines which dressed-state has the greatest overlap with the initial (ground) state, and hence has the largest occupation in the initial density matrix. This then leads to the observed directions of heat flow. Phonon absorption by laser-dressed excitons has previously been predicted by Gauger and Wabnig[49]. However, these authors investigated continuous-wave excitation, and did not address the capabilities of pulsed excitation in time-dependent thermodynamic processes as evaluated here.

Figure 2 indicates that chirping offers a significant enhancement of heat absorption. For example, for the positively detuned case shown in Fig. 2c the maximum heat for $a = 0$ is $Q/\hbar = 0.63$ ps^{-1}, at $\Theta_0 = 5.3\pi$, but maximum over the full region shown is one-and-a-half times bigger, $Q/\hbar = 0.95$ ps^{-1}. This is achieved at the boundary of the plot, $a = 40$ ps^2, $\Theta_0 = 9\pi$.

The transfer of heat from phonons to excitons which occurs over parts of Fig. 2 could be used to implement a chiller, following the thermodynamic cycle depicted in Fig. 3a. The first stroke of this cycle, shown by the solid line, is the heat absorption process discussed above. This stroke begins with the dot in its ground state, and ends in a high entropy state with temperature close to that of the phonon reservoir. This heat-absorption stroke is assumed to be short, $\tau \ll \tau_{sp}$, so that spontaneous emission can be neglected. However, the dot would then be left undriven for a time sufficient for spontaneous emission to return it to its ground state. This second process closes the cycle, which can then be repeated. The overall effect of the cycle is to extract heat from the phonon reservoir and deposit it, along with the work done by the driving laser, in the electromagnetic environment.

The focus of the present work is on the exciton-phonon heat transfer, and a detailed analysis and optimisation of the performance of the full cooling cycle has not been undertaken. However, it is interesting to estimate the cooling power. For our calculations to be valid we require $\tau_{sp} \gg \tau$, so the time for the cycle envisaged in Fig. 3a is approximately τ_{sp}. Thus the cooling power is Q/τ_{sp} (and is maximised by maximising the heat absorbed by the driving stroke, Q). The specific heat-absorption stroke depicted corresponds to a pulse with $a = 10$ ps^2, $\Theta_0 = 9\pi$, and $\tau_0 = 0.5$ ps; we refer to this pulse as the Carnot pulse, and discuss its properties further below. It gives a heat absorption of $Q/\hbar = 1.3$ ps^{-1}, which is 72% of the maximum heat that could be absorbed by the two-level system, $k_B T_{ph}$ ln 2. Taking $\tau_{sp} = 1$ ns leads to an estimated cooling power of 140 fW. We note that this is much lower than the estimate of 3 pW given by Gauger and Wabnig for their steady-state approach[49], but that should be expected because they take a much smaller $\tau_{sp} = 10$ ps.

The energy of the Carnot pulse would be 8 pJ for a dot with a transition dipole moment[52] $d = 7 \times 10^{-29}$ C m at the centre of a Gaussian beam of waist 1 μm. This is much greater than the

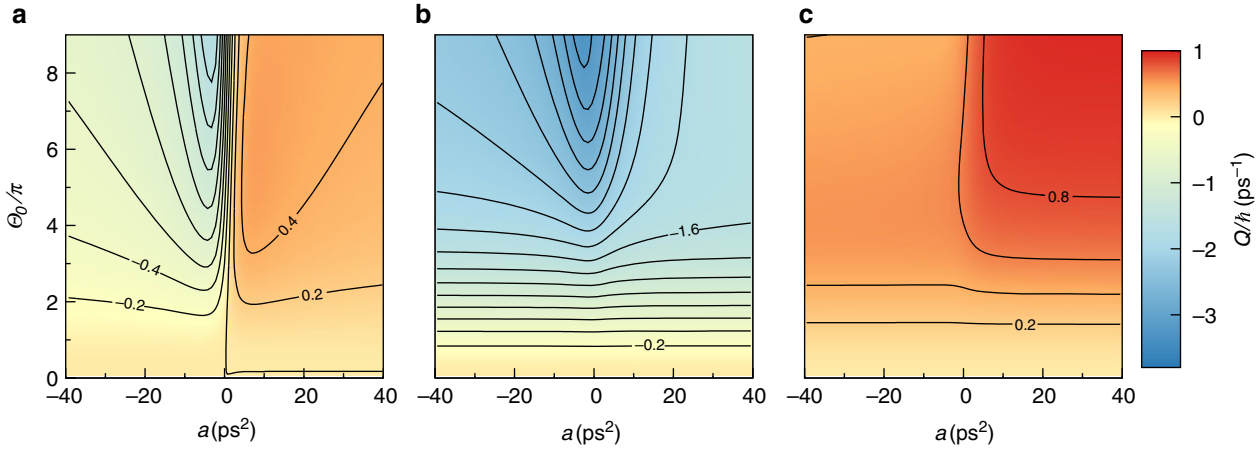

Fig. 2 Exciton-phonon heat flow for laser-driven excitons. Predicted heat absorbed, $Q/\hbar$, by a quantum-dot exciton transition, driven by a chirped laser pulse with a given spectral chirp, a, and pulse area, Θ_0. The panels correspond to different detunings between the exciton and the pulse centre frequency, $\delta = \omega_x - \omega(t=0)$. **a** $\delta = 0$. **b** $\delta = -2.5\,\mathrm{ps}^{-1}$. **c** $\delta = 2.5\,\mathrm{ps}^{-1}$. The units for the contour labels are ps^{-1} and the contour spacing is $0.2\,\mathrm{ps}^{-1}$

exciton or photon energy, and therefore also the heat absorption. The work done by the driving, which is the energy absorbed from the laser pulse, is $W = \hbar\omega_x p_x - Q \approx \hbar\omega_x p_x$, where p_x is the probability the dot is left in the excited state. For the Carnot pulse we find $p_x = 0.63$, so the cooling efficiency would be $Q/W \approx 0.1\%$ with $\hbar\omega_x = 1.5$ eV. This is very low because the energy transferred to the electromagnetic field by the spontaneous emission is wasted[53].

Heat engines and thermodynamic efficiency. We now consider the thermodynamics of the exciton-phonon heat transfer process in the context of a heat engine. This will allow us to evaluate the thermodynamic performance achievable, in a machine using such a process, in comparison to the fundamental Carnot limit. To do this we consider the thermodynamic cycle illustrated in Fig. 3b, in which heat is absorbed from the phonon reservoir at a temperature T_{ph}. For a heat engine the absorbed heat must be transferred to a reservoir at a lower temperature $T_c < T_{\mathrm{ph}}$. We suppose that this is done by a reversible process, so that the dot returns to its original state along the parts of the Carnot cycle shown by the dotted lines. Since the cycle is closed by a reversible process any departure from the Carnot efficiency can be attributed to irreversibility in the exciton-phonon heat transfer. In principle the cold stroke could be implemented using resonant electron-hole tunnelling into leads that are colder than the dot; a similar process (resonant electron tunnelling) has recently been used to implement an electronic quantum-dot heat engine[11].

Our theory allows us to calculate both the heat absorbed from the hot phonon reservoir, Q, and the entropy of the dot after the hot stroke, S. Since the initial state for the hot stroke is presumed to be the dot ground-state, with zero entropy, the cold stroke must increase the entropy of the cold reservoir by S. The heat supplied to the cold reservoir is thus T_cS, implying the work done by the cycle will be $Q - T_cS$, and the efficiency $\eta = 1 - T_cS/Q$. In the following we will take the cold reservoir temperature $T_c = 2.7$ K.

Figure 4 shows the dependence of the efficiency on the pulse area and spectral chirp, for two different unchirped pulse durations, and two different detunings. The efficiency is shown as a fraction of the Carnot efficiency at these temperatures, $\eta_c = 1 - T_c/T_{\mathrm{ph}} = 0.87$. Figure 4a gives the results for zero detuning, as is usual in an adiabatic rapid passage experiment, and $\tau_0 = 2$ ps. In this case we find a peak efficiency of $0.61\eta_c$, at a pulse area $\Theta_0 = 6.3\pi$ and spectral chirp $a = 8.0\,\mathrm{ps}^2$. Although some way below the Carnot limit this is nonetheless 80% of the Chambadal-Novikov efficiency at these temperatures, $\eta_{\mathrm{mp}} = 0.63$. Figure 4b shows the effect of introducing a positive detuning. As can be seen, this leads to considerably higher efficiencies. We note that as the chirp increases from zero to positive values the efficiency first rapidly increases, before approaching a limit. A similar behaviour is seen in the heat transfer (Fig. 2c). We believe this saturation can be attributed to the way the temporal chirp, α, and pulse duration, τ, depend on the spectral chirp, as given by Eqs. (2) and (3). In particular, for large a the temporal chirp α decreases with a, while τ increases, such that the product $\alpha\tau$ asymptotes to $1/\tau_0$.

Figure 4c, d show the corresponding results for a smaller value of τ_0, i.e., a higher bandwidth driving pulse. This leads to higher efficiencies which, for the positively-detuned case shown in Fig. 4d, reach $0.95\eta_c$. This maximum is achieved at the upper boundary of the plot $\Theta_0 = 9\pi$, in the region of positive chirp $a \gtrsim 5\,\mathrm{ps}^2$. Thus we conclude that such pulses lead to reversible exciton-phonon heat transfers.

The reversibility of the heat transfer process can also be quantified by the entropy generation. Figure 5 shows the entropy of the dot for two choices of pulse parameters. One of these, which we refer to as the Carnot pulse, corresponds to a point in Fig. 4d in the maximum efficiency region, $\Theta_0 = 9\pi$, $a = 10\,\mathrm{ps}^2$. The other, which we choose for comparison with the chirped case, is the point of maximum efficiency in Fig. 4b along the line of zero chirp ($\Theta_0 = 6.0\pi$, $\eta = 0.84\eta_c$, $Q/\hbar = 0.62\,\mathrm{ps}^{-1}$). We also plot, as the dashed line, the corresponding entropy decrease of the phonon reservoir, Q/T_{ph}, so that the gap between the two curves is the overall entropy generation. As one would expect from the difference in efficiencies, the entropy generation in the Carnot pulse is lower than that in the unchirped comparator.

Effective temperature and reversibility. To understand why some pulses induce nearly reversible heat transfers, and others do not, we consider the temperature of the dot. In general a driven system such as the dot will not be in a thermal state and, as such, will not have a well-defined temperature. Indeed in our case the exciton density matrix is not thermal in the energy eigenbasis. However, the dressed-state populations do reach thermal equilibrium with the phonons in the steady-state, because the transition rates in the dissipator obey detailed balance $\gamma_a/\gamma_e = e^{-\hbar\Lambda/k_B T_{\mathrm{ph}}}$. This relation holds more generally, suggesting that in the context of the phonon dissipation we should take the dressed-state populations, p_+ and p_-, to define the dot

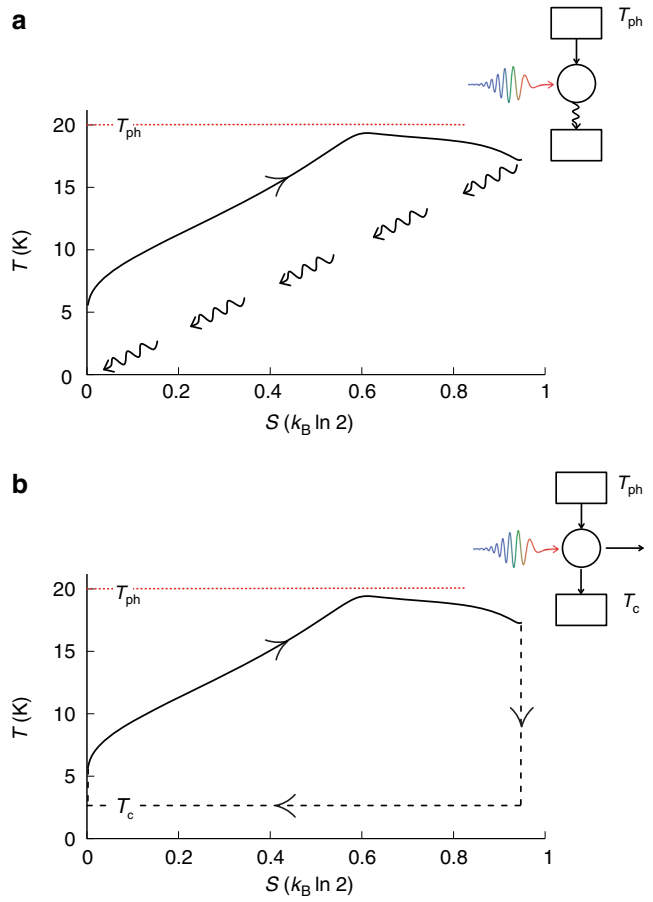

Fig. 3 Heat engines and chillers. **a** The cycle for a quantum-dot chiller. The solid curve in the temperature-entropy plot shows these quantities for the quantum-dot as it is driven by a laser pulse and absorbs heat from the phonon bath. The temperature shown is defined by Eq. (4). The wavy lines depict the subsequent radiative decay, which returns the quantum dot to its ground state. The upper (lower) square box in the engine diagram represents the phonon (electromagnetic) environment, and the circle the quantum dot. **b** The cycle for a quantum-dot heat engine. This comprises the same heat-absorption stroke as the chiller, but the cycle is then closed by a partial Carnot cycle, which implements a reversible heat transfer to a bath at a temperature $T_c < T_{ph}$

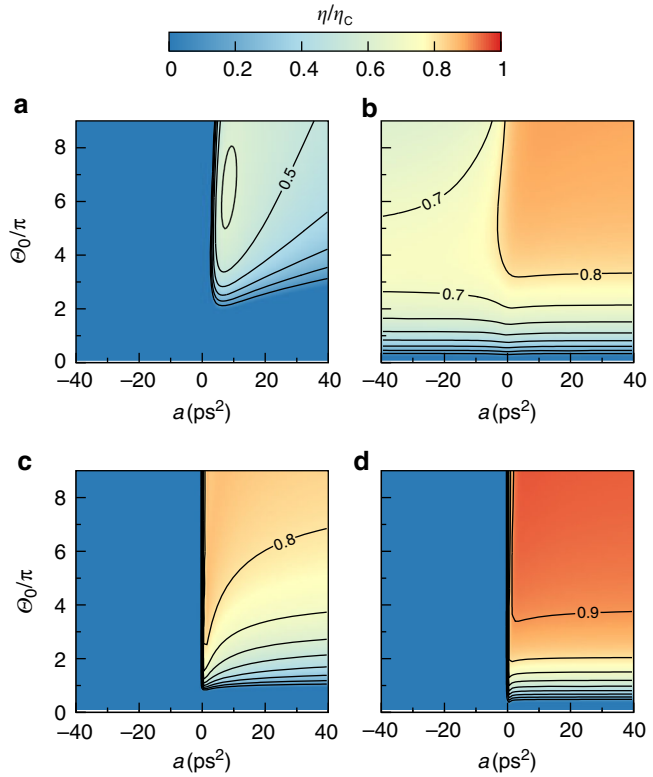

Fig. 4 Heat engine efficiency. Efficiency as a fraction of the Carnot efficiency for an exciton heat engine. Results are shown as functions of the spectral chirp (a, horizontal axes) and the pulse area (Θ_0, vertical axes) of the driving pulse used for the heat absorption stroke. The panels correspond to different values of the detuning, δ, and unchirped pulse duration, τ_0. **a** $\delta = 0$ ps^{-1}, $\tau_0 = 2$ ps^{-1}. **b** $\delta = 2.5$ ps^{-1}, $\tau_0 = 2$ ps^{-1}. **c** $\delta = 0$ ps^{-1}, $\tau_0 = 0.5$ ps^{-1}. **d** $\delta = 2.5$ ps^{-1}, $\tau_0 = 0.5$ ps^{-1}

temperature, $T_{\rm eff}$, by equating them to thermal populations,

$$p_+/p_- = e^{-\hbar\Lambda/k_B T_{\rm eff}}. \quad (4)$$

This definition of temperature is consistent with the form of the dissipator, and will allow us to interpret the entropy generation in the dissipative coupling.

Figure 6a shows the temperature of the dot, as a function of time, for the chirped Carnot pulse and the unchirped comparator pulse. We also show, in Fig. 6b, the corresponding heat currents from the phonon bath to the exciton. For the unchirped pulse the temperature of the dot, which varies during the pulse, is significantly different from that of the bath while the heat is flowing. Thus there is entropy generated throughout the process. For the chirped Carnot pulse, however, there is an interval of time during which heat flows and the temperature is constant. This is clearly an isothermal process, but it is also one in which the dot and bath temperatures are very close. It thus produces very little entropy, and is nearly reversible. This isothermal part of the heat absorption process can also be seen on the temperature-entropy plots in Fig. 3, where the solid lines are results obtained for the chirped Carnot pulse.

It may be noted that the duration of the chirped Carnot pulse, $\tau = 20$ ps, is significantly greater than that of the unchirped comparator, $\tau = 2$ ps. However, we have calculated the maximum efficiency for an unchirped pulse of these two durations, and find in both cases the same value ($0.82\eta_c$). Thus the increased duration associated with the chirping does not account for the change in efficiency.

The reversible isothermal part of the heat absorption process is made possible by the time-dependence of the dressed-state energies, which are shown for both pulses in Fig. 6c. For the chirped Carnot pulse the energy splitting is reducing during the heat transfer. This would, for an adiabatic process, reduce the temperature in line with Eq. (4). Here it compensates for the increase in temperature that would be expected as heat flows from the phonons to the exciton. The result is an isothermal heat transfer, which can occur at the bath temperature and hence be reversible. An alternative view is in terms of the scattering rates: reducing the splitting increases the ratio between phonon absorption and emission, moving the detailed-balance equilibrium for the dressed-state populations, and driving a heat flow over a negligible temperature difference.

Discussion

In this article we have shown that a theory of open quantum systems[29] can be extended to allow the calculation of quantum thermodynamic quantities. Unlike previous work[30] our theory applies to time-dependent Hamiltonians and, therefore,

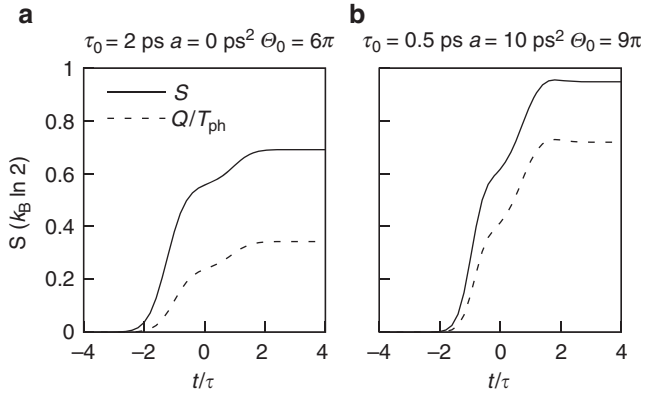

Fig. 5 Entropy changes. Entropy gained by the quantum dot (solid) and entropy lost by the phonon reservoir (dashed) as functions of time for two different driving pulses. **a** Unchirped pulse with $\delta = 2.5\,\mathrm{ps}^{-1}$ and other parameters as indicated. **b** Chirped pulse with $\delta = 2.5\,\mathrm{ps}^{-1}$ and other parameters as indicated. Time is given in units of the pulse duration, τ, in each case

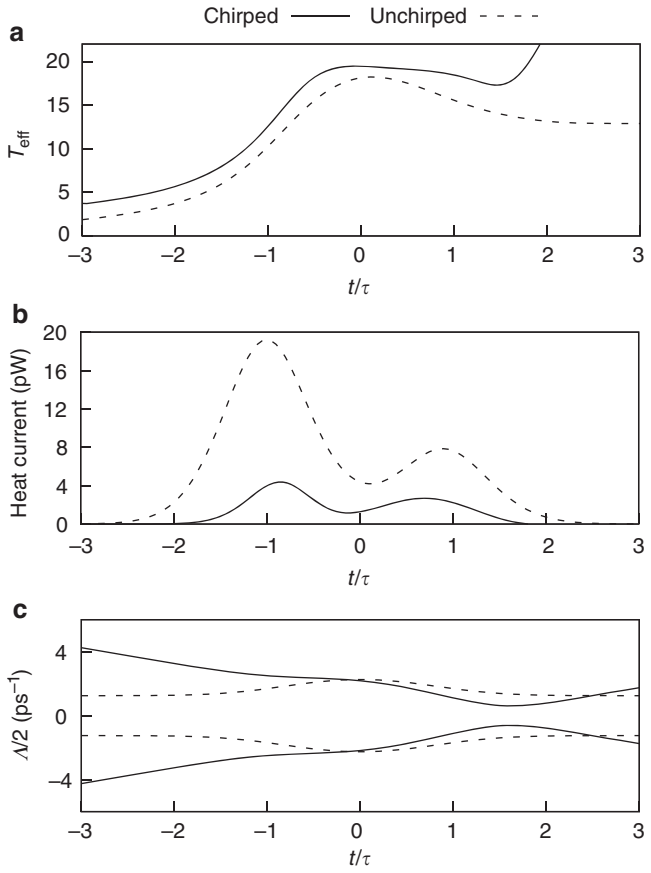

Fig. 6 Mechanism of reversible heat transfer. Results showing how chirping of the driving pulse leads to a reversible heat transfer. **a** Effective temperature of the dot as a function of time for the chirped Carnot pulse (solid) and unchirped comparator pulse (dashed). **b** Corresponding heat currents as a function of time. **c** Corresponding dressed-state frequencies, $\Lambda/2$, as a function of time. Time is given in units of the pulse duration, τ, in each case

quantum-control experiments. Using this approach we have studied the thermodynamics of a quantum-dot exciton driven by a chirped laser pulse, and evaluated the exciton-phonon heat flow, entropy generation, and effective exciton temperature during the pulse. We have predicted that certain pulses, which are readily accessible experimentally, induce heat transfers from the phonons to the excitons, and that, in some cases, this heat transfer approaches the ideal reversible limit. In the context of a heat engine such a process gives an efficiency close to the Carnot limit.

More generally, our results show that shaped laser pulses can be used to implement controlled thermodynamic processes for a single exciton transition interacting with the heat bath of phonons. The laser pulse amplitude allows for modulation of the heat flow, a feature which is essential for the implementation of thermodynamic cycles, yet is lacking in physical implementations of quantum thermodynamic machines. The pulse profile also allows simultaneous, yet independent, control over the effective temperature of the dressed-exciton system. Together, these effects allow for the implementation of any thermodynamic process in the single-qubit single-reservoir system. For example, adiabatic heating or cooling could be implemented using weak chirped pulses, for which the small pulse amplitude implies a small heat flow. These processes may be useful for high-efficiency photovoltaics, by allowing the hot excitons created by light to be cooled before they release heat. Another application of our work would be for optical cooling at low temperatures, where the freezing out of the optic phonons makes anti-Stokes cooling impossible. However, the heat absorbed in our simulations is approaching the maximum achievable for a two-level emitter, of order $k_B T_{ph}$ per cycle, and the cooling power is limited by the use of a single transition and the need for the exciton to subsequently decay, rather than by the exciton-phonon coupling. As such it would be necessary to scale to an ensemble of emitters to reach a useful cooling power, and also to reduce the radiative lifetime. This would be challenging in quantum dots, but could be explored in other optically addressable solid-state systems, such as colour centres[54].

Photon counting of exciton luminescence under pulsed excitation[25,27], or nanoscale current measurements[23,26], provides direct access to the probability distribution of the exciton occupation, and hence thermodynamic quantities such as entropy. Our theory could be tested by comparison against such experiments. Some additional thermodynamic information could be obtained optically: spectrally-resolved luminescence, for example, could give the dressed-state occupations, and hence the effective temperature. A direct measurement of the heat based on thermal effects would not be possible due to their small size. One approach could be to determine the work done by the driving pulse from its absorption, and use the first law of thermodynamics to calculate the heat. Another would be to obtain the heat from theory, fitted and validated using its predictions for quantities such as luminescence. Overall, however, the quantum-dot exciton transition seems to be a promising system in which to study thermodynamic processes at the quantum scale – given the possibility, predicted here, of using laser pulses to implement and control thermodynamic processes.

Methods

Generalised Lindblad equation. The Hamiltonian $\hat{H}_s$ may be diagonalized by introducing rotated spin operators $\hat{\mathbf{r}} = R\hat{\mathbf{s}}$, where R is a rotation by an angle $\tan^{-1}\Omega(t)/\Delta(t)$ about the y-axis. Thus $\hat{H}_s = \Lambda(t)\hat{r}_z$, implying the dressed-state energies $\pm\Lambda(t)/2$. This rotation leads to terms in the exciton-phonon coupling, $\hat{H}_c$, in which phonon emission or absorption is accompanied by transitions between the dressed states, since we have

$$\hat{s}_z = \frac{\Delta}{\Lambda}\hat{r}_z + \frac{\Omega}{2\Lambda}\left(\hat{r}_+ + \hat{r}_-\right).$$

A master equation with a dissipator corresponding to such processes has been obtained[29] by transforming to the interaction picture with respect to $\hat{H}_s + \hat{H}_b$, and applying the Born-Markov approximation to obtain a time-local equation for the reduced density matrix of the dot. Undoing the transformation to the interaction

picture, and discarding rapidly oscillating terms in the result (secularisation) gives a generalised Lindblad form, with transition operators $\hat{r}_+$ and $\hat{r}_-$, and phonon absorption and emission rates γ_a and γ_e. The coupling to $\hat{r}_z$ implies that there can be pure dephasing terms in the dressed-state basis, however, the corresponding rate is proportional to the spectral-density at zero frequency, which vanishes in this case.

Evolution of the heat distribution. To compute thermodynamic quantities, in particular the heat transferred between the phonons and the exciton, we use the generating-function or counting-field approach[55]. This approach has been previously used[30] to obtain heat and work within a Lindblad master equation, for the case of a time-independent $\hat{H}_s$. It has also been used to calculate the phonon counting statistics for an exciton with continuous-wave driving[49]. We consider the characteristic function of the heat distribution, which is a two-time correlation function of the bath energy,

$$\begin{aligned} G(u,t) &= \mathrm{Tr}\left[e^{iu\hat{H}_b}\hat{U}(t,t_0)e^{-iu\hat{H}_b}\hat{\rho}(t_0)\hat{U}^\dagger(t,t_0)\right] \\ &= \mathrm{Tr}\hat{\rho}(u,t). \end{aligned} \tag{5}$$

Here $\hat{\rho}(u,t)$ is an annotated density matrix, whose time evolution is

$$\hat{\rho}(u,t) = \hat{U}_{u/2}(t,t_0)\hat{\rho}(u,t_0)\hat{U}^\dagger_{-u/2}(t,t_0), \tag{6}$$

with the modified time-evolution operator $\hat{U}_u(t,t_0) = e^{iu\hat{H}_b}\hat{U}(t,t_0)e^{-iu\hat{H}_b}$, and $\hat{\rho}(u,t_0) = \hat{\rho}(t_0)$.

Replacing the standard time-evolution operator with the modified form in the derivation of the Lindblad master equation[29] gives the equation-of-motion for the annotated reduced density-matrix of the dot, $\hat{\rho}_s(u,t)$,

$$\begin{aligned} \frac{\partial}{\partial t}\hat{\rho}_s(u,t) = &-i\left[\hat{H}_s(t),\hat{\rho}_s(u,t)\right] \\ &-\gamma_e\left(\left\{\hat{r}_+\hat{r}_-,\hat{\rho}_s(u,t)\right\}_+ - 2e^{+iu\Lambda(t)}\hat{r}_-\hat{\rho}_s(u,t)\hat{r}_+\right) \\ &-\gamma_a\left(\left\{\hat{r}_-\hat{r}_+,\hat{\rho}_s(u,t)\right\}_+ - 2e^{-iu\Lambda(t)}\hat{r}_+\hat{\rho}_s(u,t)\hat{r}_-\right). \end{aligned} \tag{7}$$

This is a generalisation of a time-dependent Lindblad form[29] to include phase markers in the dissipator, which account in the expected way for the heat transferred in the transitions. (We drop terms corresponding to the Lamb shift, as they would have a negligible effect on our results.) It extends the result of Silaev et al.[30] to allow for time-dependence of $\hat{H}_s$, which means that the phase markers (as well as the jump operators and rates) become time-dependent due to the variation of $\Lambda(t)$.

Equation (7) is derived using the Born-Markov approximation, so that its validity requires both weak system-bath coupling, and that the bath memory time is short compared with certain timescales of the system evolution. For a time-independent $\hat{H}_s$ these timescales are the inverses of the decay rates, while the bath memory time is $1/\omega_c$, so that the approach is self-consistent when $\gamma_{a,e} \ll \omega_c$. A time-dependent $\hat{H}_s$ introduces additional relevant timescales, $H_s/\dot{H}_s$, so that the validity of the approach additionally requires $\dot{H}_s/H_s \ll \omega_c$. Technically this requirement reflects an approximation in the derivation of the dissipator, in which the full time-evolution operator, which is a time-ordered exponential, is replaced by a simpler time-local form. In addition it is necessary, in order to obtain a Lindblad form, to make the secular approximation in the dissipator, which is valid where the dynamics induced by the dissipator are slow compared with the inverse level spacing of $\hat{H}_s$. All these conditions are well satisfied in our simulations for the parameters considered here.

We have solved Eq. (7) numerically, and taken Fourier transforms of G with respect to the counting field u, to obtain the heat distributions. The results in the main text refer to the mean heat transfer, which can be computed more straightforwardly. Since the moments of the heat distribution are $\langle Q^n\rangle = \frac{1}{i^n}\frac{\partial^n G(u,t)}{\partial u^n}\Big|_{u=0}$ we find from Eq. (7) that

$$\frac{\mathrm{d}\langle Q\rangle}{\mathrm{d}t} = \Lambda(t)\left[\gamma_e(t)\rho_\uparrow(t) - \gamma_a(t)\rho_\downarrow(t)\right], \tag{8}$$

where $\rho_{\uparrow/\downarrow}(t)$ are the occupations of the dressed-states, i.e., the diagonal elements of the reduced density matrix $\hat{\rho}_s(t) = \hat{\rho}_s(u=0,t)$ in the dressed-state basis. We calculate the mean heat transferred under the driving pulse by solving Eq. (7) with $u = 0$ to obtain the occupations, and then use Eq. (8) to compute the heat. The entropy of the dot, shown in Fig. 5 and used to compute the efficiency shown in Fig. 4, is calculated from $S = -k_B\,\mathrm{Tr}\hat{\rho}_s(t)\ln\hat{\rho}_s(t)$.

Data availability

The data generated or analysed in this work are included in this published article.

Code availability

The code which generated the data used in this work is available from https://doi.org/10.5281/zenodo.326482.

Received: 11 April 2019 Accepted: 19 August 2019
Published online: 03 October 2019

References

1. Shockley, W. & Queisser, H. J. Detailed balance limit of efficiency of *p-n* junction solar cells. *J. Appl. Phys.* **32**, 510–519 (1961).
2. Fruchtman, A., Gómez-Bombarelli, R., Lovett, B. W. & Gauger, E. M. Photocell optimization using dark state protection. *Phys. Rev. Lett.* **117**, 203603 (2016).
3. Creatore, C., Parker, M. A., Emmott, S. & Chin, A. W. Efficient biologically inspired photocell enhanced by delocalized quantum states. *Phys. Rev. Lett.* **111**, 253601 (2013).
4. Dorfman, K. E., Voronine, D. V., Mukamel, S. & Scully, M. O. Photosynthetic reaction center as a quantum heat engine. *Proc. Natl Acad. Sci. USA* **110**, 2746–2751 (2013).
5. Santhanam, P., Gray, D. J. & Ram, R. J. Thermoelectrically pumped light-emitting diodes operating above unity efficiency. *Phys. Rev. Lett.* **108**, 097403 (2012).
6. Sheik-Bahae, M. & Epstein, R. I. Can laser light cool semiconductors? *Phys. Rev. Lett.* **92**, 247403 (2004).
7. Rupper, G., Kwong, N. H. & Binder, R. Large excitonic enhancement of optical refrigeration in semiconductors. *Phys. Rev. Lett.* **97**, 117401 (2006).
8. Zhang, J., Li, D., Chen, R. & Xiong, Q. Laser cooling of a semiconductor by 40 Kelvin. *Nature* **493**, 504–508 (2013).
9. van den Broeck, C. Thermodynamic efficiency at maximum power. *Phys. Rev. Lett.* **95**, 190602 (2005).
10. Abah, O. et al. Single-ion heat engine at maximum power. *Phys. Rev. Lett.* **109**, 203006 (2012).
11. Josefsson, M. et al. A quantum-dot heat engine operating close to the thermodynamic efficiency limits. *Nat. Nanotechnol.* **13**, 920–924 (2018).
12. Esposito, M., Lindenberg, K. & van den Broeck, C. Thermoelectric efficiency at maximum power in a quantum dot. *EPL* **85**, 60010 (2009).
13. Liu, Y. S. et al. A high-efficiency double quantum dot heat engine. *Appl. Phys. Lett.* **103**, 093901 (2013).
14. Jordan, A. N., Sothmann, B., Sánchez, R. & Büttiker, M. Powerful and efficient energy harvester with resonant-tunneling quantum dots. *Phys. Rev. B* **87**, 075312 (2013).
15. Ruokola, T. & Ojanen, T. Theory of single-electron heat engines coupled to electromagnetic environments. *Phys. Rev. B* **86**, 035454 (2012).
16. Vikström, A., Eriksson, A., Kulinich, S. & Gorelik, L. Nanoelectromechanical heat engine based on electron-electron interaction. *Phys. Rev. Lett.* **117**, 247701 (2016).
17. Dechant, A., Kiesel, N. & Lutz, E. All-optical nanomechanical heat engine. *Phys. Rev. Lett.* **114**, 183602 (2015).
18. Zhang, K., Bariani, F. & Meystre, P. Quantum optomechanical heat engine. *Phys. Rev. Lett.* **112**, 150602 (2014).
19. Gelbwaser-Klimovsky, D. & Aspuru-Guzik, A. On thermodynamic inconsistencies in several photosynthetic and solar cell models and how to fix them. *Chem. Sci.* **8**, 1008–1014 (2017).
20. Chen, P., Piermarocchi, C. & Sham, L. J. Control of exciton dynamics in nanodots for quantum operations. *Phys. Rev. Lett.* **87**, 067401 (2001).
21. Ramsay, A. J. A review of the coherent optical control of the exciton and spin states of semiconductor quantum dots. *Semicond. Sci. Technol.* **25**, 103001 (2010).
22. Suzuki, T. et al. Coherent control of the exciton-biexciton system in an InAs self-assembled quantum dot ensemble. *Phys. Rev. Lett.* **117**, 157402 (2016).
23. Zrenner, A. et al. Coherent properties of a two-level system based on a quantum-dot photodiode. *Nature* **418**, 612–614 (2002).
24. Ramsay, A. J. et al. Damping of exciton Rabi rotations by acoustic phonons in optically excited In GaAs/GaAs quantum dots. *Phys. Rev. Lett.* **104**, 017402 (2010).
25. He, Y.-M. et al. On-demand semiconductor single-photon source with near-unity indistinguishability. *Nat. Nanotechnol.* **8**, 213–217 (2013).
26. Wu, Y. et al. Population inversion in a single InGaAs quantum dot using the method of adiabatic rapid passage. *Phys. Rev. Lett.* **106**, 067401 (2011).
27. Simon, C.-M. et al. Robust quantum dot exciton generation via adiabatic passage with frequency-swept optical pulses. *Phys. Rev. Lett.* **106**, 166801 (2011).
28. Wei, Y.-J. et al. Deterministic and robust generation of single photons from a single quantum dot with 99.5% indistinguishability using adiabatic rapid passage. *Nano Lett.* **14**, 6515–6519 (2014).
29. Eastham, P. R., Spracklen, A. O. & Keeling, J. Lindblad theory of dynamical decoherence of quantum-dot excitons. *Phys. Rev. B* **87**, 195306 (2013).

30. Silaev, M., Heikkilä, T. T. & Virtanen, P. Lindblad-equation approach for the full counting statistics of work and heat in driven quantum systems. *Phys. Rev. E* **90**, 022103 (2014).
31. Borri, P. et al. Ultralong dephasing time in InGaAs quantum dots. *Phys. Rev. Lett.* **87**, 157401 (2001).
32. Nazir, A. & McCutcheon, D. P. S. Modelling exciton-phonon interactions in optically driven quantum dots. *J. Phys. Condens. Matter* **28**, 103002 (2016).
33. Nazir, A. Photon statistics from a resonantly driven quantum dot. *Phys. Rev. B* **78**, 153309 (2008).
34. Machnikowski, P. & Jacak, L. Resonant nature of phonon-induced damping of Rabi oscillations in quantum dots. *Phys. Rev. B* **69**, 193302 (2004).
35. Förstner, J., Weber, C., Danckwerts, J. & Knorr, A. Phonon-assisted damping of Rabi oscillations in semiconductor quantum dots. *Phys. Rev. Lett.* **91**, 127401 (2003).
36. Ramsay, A. J. et al. Phonon-induced Rabi-frequency renormalization of optically driven single InGaAs/GaAs quantum dots. *Phys. Rev. Lett.* **105**, 177402 (2010).
37. Kaldewey, T. et al. Coherent and robust high-fidelity generation of a biexciton in a quantum dot by rapid adiabatic passage. *Phys. Rev. B* **95**, 161302 (2017).
38. Schmidgall, E. R., Eastham, P. R. & Phillips, R. T. Population inversion in quantum dot ensembles via adiabatic rapid passage. *Phys. Rev. B* **81**, 195306 (2010).
39. Lüker, S. et al. Influence of acoustic phonons on the optical control of quantum dots driven by adiabatic rapid passage. *Phys. Rev. B* **85**, 121302 (2012).
40. Malinovsky, V. & Krause, J. General theory of population transfer by adiabatic rapid passage with intense, chirped laser pulses. *Eur. Phys. J. D* **14**, 147–155 (2001).
41. McCutcheon, D. P. S. & Nazir, A. Quantum dot Rabi rotations beyond the weak exciton-phonon coupling regime. *New J. Phys.* **12**, 113042 (2010).
42. McCutcheon, D. P. S., Dattani, N. S., Gauger, E. M., Lovett, B. W. & Nazir, A. A general approach to quantum dynamics using a variational master equation: application to phonon-damped Rabi rotations in quantum dots. *Phys. Rev. B* **84**, 081305 (2011).
43. Brash, A. J. et al. Dynamic vibronic coupling in InGaAs quantum dots. *J. Opt. Soc. Am. B* **33**, C115–C122 (2016).
44. Glässl, M., Barth, A. M. & Axt, V. M. Proposed robust and high-fidelity preparation of excitons and biexcitons in semiconductor quantum dots making active use of phonons. *Phys. Rev. Lett.* **110**, 147401 (2013).
45. Ardelt, P.-L. et al. Dissipative preparation of the exciton and biexciton in self-assembled quantum dots on picosecond time scales. *Phys. Rev. B* **90**, 241404 (2014).
46. Quilter, J. et al. Phonon-assisted population inversion of a single InGaAs/GaAs quantum dot by pulsed laser excitation. *Phys. Rev. Lett.* **114**, 137401 (2015).
47. Bounouar, S. et al. Phonon-assisted robust and deterministic two-photon biexciton preparation in a quantum dot. *Phys. Rev. B* **91**, 161302 (2015).
48. Liu, F. et al. Ultrafast depopulation of a quantum dot by LA-phonon-assisted stimulated emission. *Phys. Rev. B* **93**, 161407 (2016).
49. Gauger, E. M. & Wabnig, J. Heat pumping with optically driven excitons. *Phys. Rev. B* **82**, 073301 (2010).
50. Ramsey, N. F. Thermodynamics and statistical mechanics at negative absolute temperatures. *Phys. Rev.* **103**, 20–28 (1956).
51. Xi, J.-Y. & Quan, H.-T. Quantum heat engine and negative Boltzmann temperature. *Commun. Theor. Phys.* **68**, 347–356 (2017).
52. Piper, I. M. et al. Microcavity quantum-dot systems for non-equilibrium Bose-Einstein condensation. *J. Phys. Conf. Ser.* **245**, 012059 (2010).
53. Seletskiy, D. V., Epstein, R. & Sheik-Bahae, M. Laser cooling in solids: advances and prospects. *Rep. Prog. Phys.* **79**, 096401 (2016).
54. Gao, W. B., Imamoglu, A., Bernien, H. & Hanson, R. Coherent manipulation, measurement and entanglement of individual solid-state spins using optical fields. *Nat. Photon.* **9**, 363–373 (2015).
55. Esposito, M., Harbola, U. & Mukamel, S. Nonequilibrium fluctuations, fluctuation theorems, and counting statistics in quantum systems. *Rev. Mod. Phys.* **81**, 1665–1702 (2009).

Acknowledgements

This work was supported by the Irish Research Council under award No. GOIPG/2017/1091, and Science Foundation Ireland under award No. 15/IACA/3402.

Author contributions

The theory was developed and the calculations performed by C.N.M., under the supervision of P.R.E. Both authors contributed to the writing of the manuscript.

Additional information

Supplementary information accompanies this paper at https://doi.org/10.1038/s42005-019-0215-8.

Competing interests: The authors declare no competing interests.

Reprints and permission information is available online at http://npg.nature.com/reprintsandpermissions/

Publisher's note Springer Nature remains neutral with regard to jurisdictional claims in published maps and institutional affiliations.